Thyroid hormones regulate the formation and environmental plasticity of white bars in clownfishes

Pauline Salis, Natacha Roux, Delai Huang, Anna Marcionetti, Pierick Mouginot, Mathieu Reynaud, Océane Salles, Nicolas Salamin, Benoit Pujol, David Parichy, et al.

Thyroid hormones regulate the formation and environmental plasticity of white bars in clownfishes

Pauline Salis[1,2,3], Natacha Roux[1], Delai Huang[4], Anna Marcionetti[5], Pierick Mouginot[2,3], Mathieu Reynaud[6], Océane Salles[2,3], Nicolas Salamin[5], Benoit Pujol[2,3], David M. Parichy[4], Serge Planes[2,3], Vincent Laudet[6,7]*

1: Observatoire Océanologique de Banyuls-sur-Mer, UMR CNRS 7232 BIOM, Sorbonne Université Paris, 1, Avenue Pierre Fabre, 66650 Banyuls-sur-Mer, France

2: PSL Université Paris, EPHE-UPVD-CNRS, USR 3278 CRIOBE, 98729 Moorea, French Polynesia

3: Laboratoire d'Excellence "CORAIL", Perpignan, France

4: Department of Biology and Department of Cell Biology, University of Virginia, Charlottesville, Virginia 22903, USA

5: Department of Computational Biology, University of Lausanne, Lausanne, Switzerland

6: Marine Eco-Evo-Devo unit, Okinawa Institute of Science and Technology, 1919-1 Tancha, Onna son, Okinawa 904-0495 Japan.

7: Marine Research Station, Institute of Cellular and Organismic Biology (ICOB), Academia Sinica, 23-10, Dah-Uen Rd, Jiau Shi, I-Lan 262, Taïwan

*: Corresponding author: vincent.laudet@oist.jp

Keywords: Pigmentation, Developmental plasticity, Clownfishes, Thyroid Hormones, Metamorphosis

Classifications: Biological sciences- Developmental Biology

Authors contribution

P.S., N.R., M.R. and N.R. performed research. B.P., P.M. designed and performed the inference approach. D.P. and D.H. performed CRISPR-Cas9 in *D. rerio*. O.S. and S.P. performed sampling of *A. percula*. A.M. and N.S. analyzed transcriptomic data. P.S., S.P. and V.L. designed research. P.S. and V.L. wrote the article.

Abstract

Determining how plasticity of developmental traits respond to environmental conditions is a challenge that must combine evolutionary sciences, ecology and developmental biology. During metamorphosis, fish alter their morphology and color pattern according to environmental cues. We observed that juvenile clownfish (*Amphiprion percula*) modulate the developmental timing of their adult white bar formation during metamorphosis, depending on the sea anemone species in which they are recruited. We observed an earlier formation of white bars when clownfish developed with *Stichodactyla gigantea* (*Sg*) than with *Heteractis magnifica* (*Hm*). As these bars, composed of iridophores, form during metamorphosis, we hypothesized that timing of their development may be thyroid hormone (TH) dependent. We treated clownfish larvae with TH and found that white bars developed earlier than in control fish. We further observed higher TH levels, associated with rapid white bar formation, in juveniles recruited in *Sg* than *Hm*, explaining the faster white bar formation. Transcriptomic analysis of *Sg* recruits revealed higher expression of *duox*, a dual oxidase implicated in TH production as compared to *Hm* recruits. Finally, we showed that *duox* is an essential regulator of iridophore pattern timing in zebrafish. Taken together our results suggest that TH control the timing of adult color pattern formation and that shifts in *duox* expression and TH levels are associated with ecological differences resulting in divergent ontogenetic trajectories in color pattern development.

Significance statement

Developmental plasticity is defined as the ability of an organism to adjust its development depending on environmental signals, thus producing alternative phenotypes precisely adjusted to the environment. Yet the mechanisms underlying developmental plasticity are not fully understood yet. We found that juvenile clownfish delay the development of their white bars during metamorphosis, depending on the sea anemone species in which they are recruited. To understand this developmental plasticity, we investigated roles for thyroid hormones, the main hormones triggering metamorphosis in vertebrates. We found that thyroid hormones regulate white bar formation and that a shift in hormone levels, associated with ecological differences, results in divergent color patterns in different sea anemone species in which the young fish is recruited.

Introduction

Understanding the origins of biodiversity is one of the major challenges of biology, but it should not be limited to the species level, which is however already a formidable task (1). Indeed, diversity is also present within species, as phenotypic variation between distinct populations, and also within populations, depending on individual genotype and the extent to which physiology, behavior, or development are influenced by the environment (1, 2). In some instances, this phenotypic variation can reflect adaptive developmental plasticity that is defined as the ability of organisms to change their developmental trajectories to generate phenotypes precisely adjusted to the environmental conditions (1–3). Remarkable examples of such plasticity are known in animals, giving rise to distinct color patterns and other morphological traits, as well as life-histories (4). For instance, different generations of butterfly can develop alternative color patterns on their wings, depending on the season in which they emerge (5). Water fleas can grow large helmets and spikes as a response induced by predator cues, such as the concentration of kairomones in the water (6). Spadefoot toad tadpoles living in semi-arid environments accelerate their metamorphosis in response to pond drying (7).

Determining how plastic developmental changes that occur in response to environmental conditions are coordinated at the physiological, cellular, and molecular levels is a challenge that must combine ecology with developmental biology (8, 9). The mechanisms that underlie the development of alternative phenotypes are still unclear for many systems and is one major goal of ecological developmental biology or Eco-Evo-Devo (1, 10).

Pigmentation is one of the conspicuous features of animals and often has clear ecological and behavioral significance. It is thus an outstanding model for understanding links between environment and developmental plasticity. There are several cases of teleost fishes exhibiting phenotypic plasticity in pigmentation (11). This is the case in cichlids, for which several species exhibit a conspicuous yellow-blue bright phenotype linked to social dominance (12), in the platyfish in which melanic spots phenotypes are polymorphic within and among populations of *Xiphophorus variatus* depending on stress status (13), in salmonids with various pigmentation phenotypes linked to stress and social dominance (14) and also in coral reef fishes such as the dottybacks depending on the presence of prey species (15).

One of the most extraordinary life history transitions in vertebrates is metamorphosis which is regulated by thyroid hormones (TH) (16). With the very large number of TH-regulated

morphological changes occurring during larval metamorphosis (17, 18), environmentally induced alterations to TH status during this developmental period have the potential to affect outcomes of the metamorphic process (19). TH is also required to shift the larval pigmentation toward adult pattern (20). In zebrafish, for instance, TH promotes the maturation of specific pigment cells, black melanophores and yellow xanthophores (21). Whereas TH drives the terminal differentiation and proliferative arrest of melanophores, thus limiting their final number, it promotes the accumulation of orange carotenoid pigments in xanthophores, making the cells more visible (21, 22).

Here, we investigate the potential role of TH in a case of developmental plasticity in color morphs of clownfishes and we tested the impact of two environments (*e.g.* sea anemone species) on that kinetic. Among these coral reef fishes, two closely related allopatric species, *Amphiprion ocellaris* and *Amphiprion percula*, live in mutualistic symbiosis with sea anemones in the tropical Indo-pacific (23, 24). We observed that *A. percula* young juveniles (referred to here as recruits) have a different rate of white bar formation depending on the sea anemone species, their obligate symbiotic partner, in which they are recruited: white bars develop more rapidly when fish are recruited in *Stichodactyla gigantea* than in *Heteractis magnifica*. Because *A. ocellaris* acquire their adult color pattern during metamorphosis (25, 26), we asked whether developmental plasticity in bar formation is associated with alteration in TH status. Using *A. ocellaris* we found that blocking TH production delayed white bar formation, whereas excess TH accelerated white bar formation, revealing a role for TH in determining the rate at which color pattern shifts from larva to juvenile form. To test the ecological significance of these findings, we assayed TH titers and gene expression in wild-caught *A. percula* and found that young recruits associated with *S. gigantea* exhibited a higher levels of TH and more abundant transcript of *duox*, a gene implicated in thyroid function and TH synthesis, as compared to recruits associated with *H. magnifica* (27). Further supporting a role for *duox* and TH in regulating the timing of iridophore patterning, we found that zebrafish deficient for *duox* activity were delayed in iridophore stripe formation relative to overall developmental progression. Taken together our results suggest that TH regulates color pattern formation in clownfish and that shifts in hormone levels are associated with ecological differences that result in divergent ontogenetic trajectories in color pattern formation.

Results

Formation of white bars of *A. percula* new recruits is differentially influenced by age or size depending on anemone species

Amphiprion species acquire, in sequence, the head, body and finally peduncle white bars during post-embryonic development (26). In Kimbe bay, Papua New Guinea, *A. percula* is found in two different sea anemone hosts, *Stichodactyla gigantea* and *Heteractis magnifica* and the fish leaving in these two hosts belongs to the same population (28). We observed in the field that new *A. percula* recruits in *S. gigantea* have more white bars than new recruits in *H. magnifica* for juveniles of the same age and developmental stage (juvenile stage). In fact, 33% of 148 new recruits (200–250 days old) in *S. gigantea* had 3 white bars, whereas only 5% of 118 new recruits of the same age in *H. magnifica* had this pattern (Fig. 1 A and B, Test χ^2 p-value=0.0011).

We tested by multiple regression whether sea anemone species affects the timing of white bar formation of *A. percula* new recruits from Kimbe bay, while accounting for ecological and social structure variables. These results confirm our observations that new recruits had consistently more bars in *S. gigantea* than in *H. magnifica* for a similar age or size (Fig. 1C and D, Supp Fig 1A and B and Supp Table 1-4).

As illustrated Fig. 1C and Supp. Fig. 1A, the speed at which bands were acquired varies with age (or with size) and how the acceleration and deceleration of band acquisition varied with age (or size) also depends of the anemone species. Thus, our results indicate that anemone species differentially modulate the dynamic to which bars were acquired with age (or size). In fact, available data allow us to detect differences between anemone species in the shape of the relationship between bars and age (or size), but more data would be needed to fully characterize the shape of these relationships.

Adult color pattern formation is linked to a switch in pigment cell specific gene expression

Because we know that the sister species, *A. ocellaris* acquire their adult color pattern during metamorphosis (25, 26), we addressed whether TH is associated with developmental plasticity in color pattern using this species as a laboratory model (24, 25). *A. ocellaris* exhibits two pigmentation patterns during development: before stage 5 (around 9 dph; (25)), larvae have yellow larval xanthophores with a set of stellate larval melanophores forming two horizontal stripes covering the myotomes (Fig. 2A, B, C and D, red arrowheads). From stage

5, larvae acquire, in a rostro-caudal temporal gradient, three white vertical bars (Fig. 2E, F, G, white arrowheads), orange xanthophores outside of the future white bars (Fig. 2E, orange arrows) and melanophores dispersed all over the body (Fig. 2E and F, black arrows) (25, 29). These melanophores are present over the body and are at higher density at the border of the white bars (Fig. 2F and G).

To better understand color pattern changes occurring around stage 4, we assessed the expression of pigmentation genes across post-embryonic stages. We extracted RNA from whole larvae at each of the seven *A. ocellaris* post-embryonic stages and performed transcriptomic analysis (29). We focused on pigmentation genes defined by (30, 31) (Fig. 2H, Supp Fig. 2A and Supp Table 5), and particularly on iridophore genes, as we showed previously that white bars are formed by iridophores (29) (Fig. 2I and J and Supp Table 5). We observed that stages 1 to 3 are clearly separated from stages 4 to 7 along principal component 2 (PC2) (Fig. 2 H and I). Among those genes, *fhl2b, pnp4a* and *prkacaa* have a highest fold difference at stages 5 to 7 compared to stages 1 to 3 whereas *gbx2, trim33, gmps* and *oca2* have a highest fold difference at stages 1 to 3 compared to stages 5 to 7 (Fig. 2J). We also observed a clear separation across stages for all the functional categories described in (30) (Supp Fig. 2A): pigment cell specification (Supp Fig. 2B), xanthophore development (Supp Fig. 2C), pteridine pigment synthesis of xanthophores (Supp Fig. 2D), as well as melanophore development (Supp Fig. 2E), melanogenesis regulation (Supp Fig. 2F), and at a later stage, melanosome biogenesis (Supp Fig. 2G).These outcomes are consistent with changes across stages in pigmentation gene expression, complements of different pigment cell types, or likely both. They suggest that an important switch in the development of color pattern, involving each of the three pigment cells, occurs at stage 4.

White bar formation is controlled by thyroid hormone signaling

TH contributes to metamorphosis and the developmental program controlling pigmentation pattern in zebrafish and other teleosts (21, 32, 33). We hypothesized that TH regulates the timing of white bar formation during clownfish metamorphosis. To test this hypothesis, we exposed stage 3 larvae (5 dph) to different concentrations (10^{-6}, 10^{-7} and 10^{-8} M) of the active thyroid hormone, T3. After 3 days of treatment with T3, we observed a more rapid appearance of white bars than in control larvae. This effect was dose-dependent with, at 3 days post-treatment (dpt), 0 % of the fish exhibiting two bands in the control, 50% at 10^{-8} M T3, 78% at 10^{-7} M and 73% at 10^{-6}M (Fig. 3A to D; Fig. 3E).

We then tested the effect of decreasing TH signaling by blocking TH production with a mix of goitrogens (34). Larvae treated from stage 3 (5 dph) had a delay in white bar development compared to controls at 9 dpt (Fig. 3H compared to the control Fig. 3G; Fig. 3F): whereas 75% of controls had developed head and trunk white bars, only 15% of larvae treated with

MPI (Methimazol, Perchlorate Potassium and Iopanoïc Acid) exhibited these bars and the remainder were devoid of any bars (Fig. 3F). It should be noted that after 25 days of treatment, white bars ultimately formed in MPI-treated fishes demonstrating that a delay, rather than blockade in bar formation is associated with TH inhibition (Fig. 3I).

Pigment cells other than iridophores were also affected by TH treatment, with melanophore numbers increasing significantly within 48 h of treatment with 10^{-6} M T3 beginning at stage 3 (5 dph) (Fig. 3J- $p\text{-value}_{48hpt} = 0.0299$; $p\text{-value}_{72hpt} = 0.0043$). In contrast, MPI treatments led only to a minor decrease (non-significant) in melanophore numbers at 48 or 72 hpt (Fig. 3J). We did not observe gross differences in xanthophore development, and it was not possible to identify individual xanthophores or to quantify their numbers.

Taken together, these results suggest that TH controls the timing of white bar formation relative to overall somatic development and may act on iridophores and melanophores.

Expression of pigmentation genes is modified by T3 treatment

To determine how TH affects iridophores, we assayed expression of iridophore genes (*fhl2a*, *fhl2b*, *apoda.1*, *saiyan* and *gpnmb; 27)* after treating larvae with exogenous TH. Stage 3 larvae were treated with T3 at different concentrations (10^{-6}, 10^{-7} and 10^{-8} M) for 12, 24, 48 and 72 hours and expression of these genes was monitored by nanostring in RNA extracted from whole larvae. After T3 treatment, transcripts for all of these genes were significantly more abundant compared to levels in controls (Supp Fig. 3). In some cases (*apod1a* and *gpnmb*) this effect was evident by 12h and in others (*fhl2a*, *fhl2b* and *saiyan*) only after 24 or 48h. This suggests that TH affects expression of genes known to be expressed in clownfish iridophores.

Treatments with thyroid hormones or goitrogens lead respectively to ectopic iridophores over the body and decrease in white hue in white bars

To determine whether TH promotes iridophore differentiation, we treated stage 3 larvae with T3 at 10^{-6} M for a longer period to compare juveniles at stage 6, when fish have developed both head and body bars. Interestingly, head and body bars were never fully formed in T3 treated juveniles compared to controls (Supp Fig. 4D compared to Supp Fig. 4A) and close inspection of larvae revealed numerous ectopic iridophores across the flank of T3 treated fish (Supp Fig. 4F compared to Supp Fig. 4C- white arrowheads). Moreover, orange coloration was decreased in T3 treated juveniles compared to control (compare Supp Fig. 4B and Supp Fig. 4E). MPI treatment led to bars with normal shapes that were, nevertheless, more translucent presumably owing to deficiencies in the numbers of iridophores or the deposition of crystalline guanine within iridophores normally responsible for their white (or iridescent) appearance (N=2, Fig. 3I).

Together, these results indicate that exogenous TH leads to reduced orange coloration and defects in white bar formation accompanied by ectopic iridophores on the body, whereas blockade of TH production leads to a reduced number of white iridophores or reflective guanine within white bars.

Ecological modulation in timing of white bar formation is linked to TH levels and *duox* expression.

As TH treatment accelerated white bar development in *A. ocellaris*, we asked whether the accelerated acquisition of bars in *A. percula* recruits in *S. gigantea* was linked to TH. We sampled a second set of new recruits of 12-27 mm (having one white bar either complete or being formed) living either in *S. gigantea* (N=6) or *H. magnifica* (N=6) and measured TH levels. Concentrations of T3 (in pg/ g of larvae) were significantly greater in new recruits sampled from *S. gigantea* compared to the those from *H. magnifica* (Fig. 4A).

To gain insight into mechanisms that explain these differences we compared gene expression between *A. percula* new recruits found in *H. magnifica* (n=3) or *S. gigantea* (n=3) by RNA-Seq of whole fish. Out of the 19063 analyzed genes, only 21 were significantly more expressed in new recruits from *S. gigantea* (adj. *P*-value < 0.05, $Log_2FC > 1$), while 15 were significantly more expressed in new recruits from *H. magnifica* (adj. *P*-value < 0.05, $Log_2FC < 1$) (Fig. 4B, Supp. table 6). Within the differentially expressed genes, we observed *duox,* which encodes a dual oxidase implicated in TH production (27, 35). This gene was significantly overexpressed in new recruits from *S. gigantea* (adj. *P*-value = 0.038, $Log_2FC = 2.53$) compared to those from *H. magnifica*. Together, these results suggest that the rate of white bar formation in *A. percula* is linked to a differential level of T3, which is in turn linked to a differential expression of *duox*.

Last, we wanted to directly test whether *duox* is required for iridophore patterning. For this we used zebrafish *Danio rerio*, in which iridophores depend on TH for their maturation (22). *duox* requirements have been described for somatic development and melanophore numbers, but not iridophore pattern (27, 35). We therefore injected one-cell stage embryos of the iridophore reporter line Tg(*pnp4a:palm-mcherry*)^{wprt10Tg} with highly efficient Alt-R CRISPR-Cas9 (36) targeting *duox*, resulting in phenotypes concordant with those for this locus (27, 35) and other hypothyroid fish (21, 22). Figure 4C shows mCherry+ iridophores (dark cells; pixel values inverted) in representative uninjected (wild-type) and *duox*-deficient larvae of the same stage [10.6 mm standard length (SL)]. In wild-type, densely packed iridophores have formed one complete interstripe and a second interstripe has started to form ventrally; some

loosely arranged iridophores occur in between, where a melanophore stripe develops (37). In the *duox*-deficient larva only a single wider interstripe has developed and fewer stripe iridophores are visible (Fig. 4C) suggesting that iridophore development is slowed in *duox*-deficient animals. Consistent with this interpretation, most wild-type fish greater than 11.0 mm SL had developed two complete interstripes (score=2.0), whereas equivalently staged *duox*-deficient fish had developed only one complete interstripe and were still developing a second interstripe (score=1.5) (Fig. 4D). Despite having fewer interstripes overall, *duox*-deficient animals had proportionally more of the flank covered by dense, interstripe iridophores, as compared to the wild type (Fig. 4E). These data show that *duox*, presumably acting through TH (27, 35), contributes to the timing of iridophore interstripe appearance and the patterning of interstripes in zebrafish.

To conclude, our findings suggest that reduced abundance of *duox* transcript in *A. percula* recruits within *H. magnifica* in comparison with those that are recruited in *S. gigantea* leads to a delay in the development of their white bars. This effect of *duox* in regulating the timing of iridophore development is conserved between the distantly related clownfish and zebrafish.

Discussion

During post-embryonic development, *A. ocellaris* lose their larval color pattern and acquire in a few days and in a rostro-caudal sequence the head, body and caudal peduncle white bars of their final adult color pattern. We showed here that during clownfish metamorphosis the formation of iridophore-containing white bars that are formed by iridophores is accelerated by TH, and that TH also underlie environmental (*e.g.* sea anemone species) plasticity in bar formation in wild populations. Interestingly a corresponding effect on iridophore patterning was also seen in zebrafish: *duox* mutants are hypothyroid (27, 35), and we found that iridophore patterning of *duox*-deficient animals was delayed. All these data converge toward the notion that variations in TH levels control a plastic pigmentation phenotype observed in clownfishes.

The observation that in both clownfish and zebrafish, TH affects white bar (clownfish) or interstripe (zebrafish) formation strongly suggests that these hormones directly or indirectly act on iridophores. Previous studies revealed that TH deficiency in zebrafish leads to an excess of melanophores and a loss of visible xanthophores (21). Further analyses showed that these hormones act differently on these two cell types, promoting maturation but via distinct mechanisms. TH promotes terminal differentiation and limits the final number of melanophores whereas it promotes accumulation of carotenoid pigments in xanthophores, making initially unpigmented precursors visible. A similar role for TH in promoting iridophore maturation was suggested by analyses of single cell transcriptomic states, though consequences for iridophore number and pattern were not assessed (22). In our analysis we observed that interstripe development is slowed in *duox*-deficient animals and that *duox*-deficient animals had proportionally more of the flank covered by dense, interstripe-iridophores, as compared to the wild type. Together these several observations support the idea that TH signaling has an evolutionarily conserved role in regulating the timing of iridophore development in two species having markedly different adult pigment patterns. TH receptors are expressed in iridophores of both species but analyses to date cannot indicate whether effects of TH are direct or mediated through other cell types (22).

We also observed an effect of TH on the shape of the trunk white bars in clownfish. Indeed, late in TH treated fishes, we observed abnormalities in this trunk white bar that is misshapen and incomplete (*e.g.* it does not cross the full body of the fish; see Supp Figure 4D). This is interesting as a similar phenotype is often observed in clownfish juveniles raised in the

laboratory and has been assumed to result from nutritional defects (38–40). In addition to abnormalities in the shape of white bars, we observed ectopic iridophores. We cannot exclude at this point that the defects in white bar shape could be linked to a role of TH on pigment cells migration.

We have observed that *A. percula* developing in association with *S. gigantea* acquire white bars and have higher levels of T3, than *A. percula* in *H. magnifica*. This difference can be explained by higher expression of *duox* by *A. percula* recruited in *S. gigantea* as compared to *A percula* recruited in *H. magnifica*. Indeed, *duox*, encodes a dual oxidase that has been implicated in TH production both in mammals and zebrafish (27, 35). Beyond the effects of *duox* inactivation we observed on zebrafish iridophore patterning, duox mutants have growth retardation, ragged fins, thyroid hyperplasia and infertility and, a pigmentation phenotype with increased melanophore and reduced xanthophore (27, 35) typical of hypothyroid fish (21). As shown by Chopra *et al.*, some of these defects can be rescued with T4 treatment, even when initiated in adult fish (27). All these data allow us to suggest that in young juveniles which are recruited in *S. gigantea* there is an increased expression of *duox* that led to a higher TH level and a higher rate of white bar formation.

The results of our study leave two major questions unanswered: why is there an increased *duox* expression in *S. gigantea* recruits, and is there ecological significance to faster white bar formation in those fish. The regulation of *duox* gene expression in fish is still poorly known but it has been shown that *Duox1* and *Duox2* expression in mammals in tightly controlled and regulated by TSH, that is the hypothalamo-pituitary-thyroid axis (41). As *S. gigantea* has been shown to be a much more toxic sea anemone than *H. magnifica* by hemolytic and neurotoxicity assays (42), it is conceivable that clownfish recruited in this sea anemone perceive this harsher environment and hence activate their neuroendocrine axis to compensate. It is important to note in that respect that several anemonefish adults (*A. percula* but also *A. clarki*, *A. polymnus* or *A. chrysopterus*) exhibit a similar polymorphic melanistic morph when present in *Stichodactyla* vs. *Heteractis* (43). It is tempting to propose that these melanistic morphs are also linked to TH signaling in these species. The white bar phenotype we discussed here is therefore likely to be only one of a series of changes linked to the differential recruitment in various sea anemone species that allow the physiological adjustment of the fish in these distinct environments (44). However, the adaptative significance of this plastic phenotype is still only a hypothesis that remains to be tested experimentally in the field (44). It is interesting to note that *A. ocellaris* can also live in the same two sea anemone species but does not exhibit a melanistic morph when present in *Stichodactyla* (45). The rate of white bar appearance in young recruits of *A. ocellaris* living in the two sea anemone species is unknown. It will be interesting to study in the future the

differences in pigmentation plasticity between the two sister species, *A. ocellaris* and *A. percula*.

In conclusion, our study of white bar formation in clownfish highlight the interest of this new emerging system to investigate the cellular, molecular endocrine and developmental basis of alternative phenotypes that are detected in natural situation (24, 46). Combining analysis in the wild as well as in the lab, as we have done here using clownfish as model, offers great promises to understand the evolutionary and developmental basis of plastic phenotypes often observed in nature.

Acknowledgments

This study was supported by Agence Nationale de la Recherche (ANR-19-CE34-0006-Manini and ANR-19-CE14-0010-SENSO) as well as by National Institute of Science (NIH R35 GM122471). We thank Valentin Logeux, Remi Pillot, Nancy Trouillard and Pascal Romans from the Aquariology Service at Observatoire Océanologique de Banyuls-Sur-Mer for expert technical help for clownfish husbandry. We also thank the Centre de Recherches en Cancérologie de Toulouse (CRCT UMR 1037 INSERM, Plateau Génomique et Transcriptomique) for the Nanostring experiments.

Materials and methods

See extended methods provided in *SI Appendix*.

***A. ocellaris* larval rearing and ethics**. *A. ocellaris* were maintained as described in (25). We have approval for these experiments from the C2EA - 36 Ethics Committee for Animal Experiment Languedoc-Roussillon (CEEA-LR), number A6601601. The experimental protocols were following French regulation.

RNA extraction and transcriptomic analysis. Transcriptomic data of developmental stages of *A. ocellaris* larvae were taken from the transcriptomic analysis of *A. ocellaris* post-embryonic stages performed in (29). For more information see *SI Appendix*. Individuals of *A. percula* new recruits were sampled, euthanized in a MS222 solution (200 mg/l) and conserved in RNAlater. Total RNA of each individual was extracted using (Trizol Reagent 15596-026 kit, Ambion) followed by DNase treatment (DNA-free AM1906 kit, Ambion) and then purified with 0.025 µm dialysis membranes. RNA-Seq libraries and sequencing were performed on a Illumina HiSeq4000 sequencer using a stranded protocol as Paired-end 50 base reads. Transcriptomic analysis is described in *SI Appendix*.

Drug treatment of *A. ocellaris* larvae. T3 (3,3',5-Triiodo-L-thyronine) and IOP (Iopanoic Acid) were both diluted in dimethylsulphoxyde (T3: T2877, IOP: 14131, DMSO: D8418; Sigma-Aldrich Louis, MI, USA) to a final concentration 1 mM. To analyze the effect of a reduction of TH signaling we used a mix of goitrogens called MPI (Methimazole, Potassium Perchlorate and Iopanoic Acid) as in reference (47). Methimazole, Potassium Perchlorate and IOP (Methimazole: M8506, Potassium perchlorate 460494, Sigma-Aldrich Louis, MI, USA) were also diluted in DMSO to a respective final concentration of 100 mM, 10 mM and 1 mM. Larvae were treated from 5 until 18 dph in 0.005% DMSO with T3+IOP at 10^{-6}, 10^{-7} and 10^{-8} M (respective dilutions of 1/1000, 1/10000 or 1/100000) or MPI (dilution of 1/1000) or without (controls). For each condition, five larvae were treated in 500-mL fish medium in a beaker. One hundred milliliters of solution were changed every day.

Nanostring gene expression analysis. 400 ng of total RNA were analyzed using the Nanostring Counter. Each sample was analyzed in a separate multiplexed reaction including 8 negative probes and 6 serial concentrations of positive control probes. Data were imported

into nSolver software (version 2.5) for quality checking and data normalization according to NanoString guidelines. Analysis was done using the R package TTCA1 (R version 3.5.1).

Effect of ecological factors on the number of bars in new recruits of *A. percula*. At the time of the sampling in Kimbe bay (5°12′22.56″ S, 150°22′35.58″ E), West New Britain Province, Papua New Guinea, we characterized the new recruit size, age (see SI appendix) ecological variables (geographic zone, primary host anemone species, depth), and the social structure of the new recruits within its sea anemone (total number of conspecifics inhabiting the sea anemone, size difference between the new recruit and the last subadult in the social hierarchy, female size) (28, 48). In the studied *A. percula* colonies located in Kimbe 43% are in *S. gigantea* and 57% in *H. magnifica*. To assess what factors affect the number of bars on new recruits, we modelled the number of bars as a response variable depending upon either size or age, their squared value, and ecological and social structure independent variables. We followed a multi-model inference approach (49, 50) to estimate predictors effect sizes and their 85% confidence interval (51). This approach was conducted independently in each anemone species to avoid confounding effects between anemone species and depth (see Supp. Methods for details of the statistical analysis). All analyses were performed with the MuMIn v1.43.6 package (52) in the statistical software R v3.6.3 (53).

Thyroid hormones extraction and dosage. TH were extracted individuals from *A. percula* new recruits sampled in Kimbe Island, dry-frozen (previously euthanized in a 200 mg/l solution of MS-222) following the protocol described in (32). More details are described in *SI Appendix*.

Zebrafish duox CRISPR-Cas9. Zebrafish *D. rerio* were reared under standard conditions (28 °C, 14L:10D) and staged according to (54). Embryos Tg(*pnp4a:palm-mcherry*)^{wprt10Tg} expressing membrane-targeted mCherry (mem-Cherry) (55, 56) were injected at the one-cell stage with Alt-R CRISPR-Cas9 (36) targeting *duox*, and reared on a thyroid hormone free diet of brine shrimp and marine rotifers (21). Images of *duox* AltR-injected fish and uninjected controls were acquired on a Zeiss Axio Observer inverted microscope equipped with a Yokogawa CSU-X1M5000 laser spinning disk with Hamamatsu ORCA-Flash 4.0 camera. Regions of interest were defined by the anterior and posterior margin of the anal fin, and proportional coverage of dense interstripe iridophores relative to this region of interest were analyzed using ImageJ software. Numbers of completed or developing interstripes were scored qualitatively. Display levels were adjusted and inverted for visualization in Adobe Photoshop 2021.

References

1. M. J. West-Eberhard, Developmental plasticity and the origin of species differences. *Proc. Natl. Acad. Sci.* **102**, 6543–6549 (2005).
2. O. Leimar, Environmental and genetic cues in the evolution of phenotypic polymorphism. *Evol. Ecol.* **23**, 125–135 (2009).
3. B. Taborsky, *Developmental Plasticity: Preparing for life in a complex world* (Elsevier Ltd, 2017).
4. D. W. Pfennig, *et al.*, Phenotypic plasticity's impacts on diversification and speciation. *Trends Ecol. Evol.* **25**, 459–467 (2010).
5. H. F. Nijhout, Development and evolution of adaptive polyphenisms. *Evol. Dev.* **5**, 9–18 (2003).
6. E. Hammill, A. Rogers, A. Beckerman, Costs, benefits and the evolution of inducible defences: a case study with Daphnia pulex. *J. Evol. Biol.* **21**, 705–715 (2008).
7. S. S. Kulkarni, R. J. Denver, I. Gomez-Mestre, D. R. Buchholz, Genetic accommodation via modified endocrine signalling explains phenotypic divergence among spadefoot toad species. *Nat. Commun.* **8**, 993 (2017).
8. S. F. Gilbert, Mechanisms for the environmental regulation of gene expression: ecological aspects of animal development. *J. Biosci.* **30**, 65–74 (2005).
9. N. Aubin-Horth, S. Renn, Genomic reaction norms: using integrative biology to understand molecular mechanisms of phenotypic plasticity. *Mol. Ecol.* **18**, 3763–3780 (2009).
10. S. F. Gilbert, D. Epel, *Ecological Developmental Biology: The Environmental Regulation of Development, Health and Evolution.* Sinauer Associates (2015) pp. 576.
11. A. C. Price, C. J. Weadick, J. Shim, F. H. Rodd, Pigments, patterns, and fish behavior. *Zebrafish* **5**, 297–307 (2008).
12. P. D. Dijkstra, *et al.*, The melanocortin system regulates body pigmentation and social behaviour in a colour polymorphic cichlid fish. *Proc. R. Soc. B Biol. Sci.* **284**, 20162838 (2017).
13. Z. W. Culumber, Variation in the evolutionary integration of melanism with behavioral and physiological traits in Xiphophorus variatus. *Evol. Ecol.* **30**, 9–20 (2016).
14. L. Jacquin, *et al.*, Melanin in a changing world: brown trout coloration reflects alternative reproductive strategies in variable environments. *Behav. Ecol.* **28**, 1423–1434 (2017).
15. F. Cortesi, *et al.*, Phenotypic plasticity confers multiple fitness benefits to a mimic. *Curr. Biol.* **25**, 949–954 (2015).

16. V. Laudet, The origins and evolution of vertebrate metamorphosis. *Curr. Biol.* **21**, R726–R737 (2011).
17. S. K. McMenamin, D. M. Parichy, “Metamorphosis in Teleosts” in *Current Topics in Developmental Biology*, (2013), pp. 127–165.
18. M. A. Campinho, Teleost metamorphosis: the role of thyroid hormone. *Front. Endocrinol. (Lausanne).* **10** (2019).
19. S. C. Lema, Hormones, developmental plasticity, and adaptive evolution: Endocrine flexibility as a catalyst for ‘plasticity-first’ phenotypic divergence. *Mol. Cell. Endocrinol.* **502**, 110678 (2020).
20. L. B. Patterson, D. M. Parichy, Zebrafish Pigment Pattern Formation: Insights into the Development and Evolution of Adult Form. *Annu. Rev. Genet.* **53**, 505–530 (2019).
21. S. K. McMenamin, *et al.*, Thyroid hormone-dependent adult pigment cell lineage and pattern in zebrafish. *Science (80-.).* **345**, 1358–1361 (2014).
22. L. M. Saunders, *et al.*, Thyroid hormone regulates distinct paths to maturation in pigment cell lineages. *Elife* **8** (2019).
23. G. Litsios, *et al.*, Mutualism with sea anemones triggered the adaptive radiation of clownfishes. *BMC Evol. Biol.* **12**, 212 (2012).
24. N. Roux, P. Salis, S.-H. Lee, L. Besseau, V. Laudet, Anemonefish, a model for Eco-Evo-Devo. *Evodevo* **11**, 20 (2020).
25. N. Roux, *et al.*, Staging and normal table of postembryonic development of the clownfish (Amphiprion ocellaris). *Dev. Dyn.* **248**, 545–568 (2019).
26. P. Salis, *et al.*, Ontogenetic and phylogenetic simplification during white stripe evolution in clownfishes. *BMC Biol.* **16**, 90 (2018).
27. K. Chopra, S. Ishibashi, E. Amaya, Zebrafish duox mutations provide a model for human congenital hypothyroidism. *Biol. Open* **8**, bio037655 (2019).
28. O. C. Salles, *et al.*, First genealogy for a wild marine fish population reveals multigenerational philopatry. *Proc. Natl. Acad. Sci.* **113**, 13245–13250 (2016).
29. P. Salis, *et al.*, Developmental and comparative transcriptomic identification of iridophore contribution to white barring in clownfish. *Pigment Cell Melanoma Res.* **32**, 391–402 (2019).
30. T. Lorin, F. G. Brunet, V. Laudet, J.-N. Volff, Teleost fish-specific preferential retention of pigmentation gene-containing families after whole genome duplications in Vertebrates. *G3; Genes|Genomes|Genetics* **8**, 1795–1806 (2018).
31. I. Braasch, F. Brunet, J.-N. Volff, M. Schartl, Pigmentation pathway evolution after whole-genome duplication in fish. *Genome Biol. Evol.* **1**, 479–493 (2009).
32. G. Holzer, *et al.*, Fish larval recruitment to reefs is a thyroid hormone-mediated metamorphosis sensitive to the pesticide chlorpyrifos. *Elife* **6** (2017).

529 33. Y. Inui, S. Miwa, Thyroid hormone induces metamorphosis of flounder larvae. *Gen.*
530 *Comp. Endocrinol.* **60**, 450–454 (1985).
531 34. S. Remaud, *et al.*, Transient hypothyroidism favors oligodendrocyte generation
532 providing functional remyelination in the adult mouse brain. *Elife* **6** (2017).
533 35. J.-S. Park, *et al.*, Targeted knockout of duox causes defects in zebrafish growth,
534 thyroid development, and social interaction. *J. Genet. Genomics* **46**, 101–104 (2019).
535 36. K. Hoshijima, *et al.*, Highly efficient CRISPR-Cas9-based methods for generating
536 deletion mutations and F0 embryos that lack gene function in zebrafish. *Dev. Cell* **51**,
537 645-657.e4 (2019).
538 37. D. Gur, *et al.*, In situ differentiation of iridophore crystallotypes underlies zebrafish
539 stripe patterning. *Nat. Commun.* **11**, 6391 (2020).
540 38. J. G. Eales, The influence of nutritional state on thyroid function in various vertebrates.
541 *Am. Zool.* **28**, 351–362 (1988).
542 39. D. S. MacKenzie, C. M. VanPutte, K. A. Leiner, Nutrient regulation of endocrine
543 function in fish. *Aquaculture* **161**, 3–25 (1998).
544 40. K. A. Leiner, D. S. Mackenzie, Central regulation of thyroidal status in a teleost fish:
545 Nutrient stimulation of T4 secretion and negative feedback of T3. *J. Exp. Zool.* **298A**,
546 32–43 (2003).
547 41. M. Milenkovic, *et al.*, Duox expression and related H2O2 measurement in mouse
548 thyroid: onset in embryonic development and regulation by TSH in adult. *J. Endocrinol.*
549 **192**, 615–626 (2007).
550 42. A. M. Nedosyko, J. E. Young, J. W. Edwards, K. Burke da Silva, Searching for a Toxic
551 Key to Unlock the Mystery of Anemonefish and Anemone Symbiosis. *PLoS One* **9**,
552 e98449 (2014).
553 43. T. A. Militz, M. I. McCormick, D. S. Schoeman, J. Kinch, P. C. Southgate, Frequency
554 and distribution of melanistic morphs in coexisting population of nine clownfish species
555 in Papua New Guinea. *Mar. Biol.* **163**, 200 (2016).
556 44. A. Ducrest, L. Keller, A. Roulin, Pleiotropy in the melanocortin system, coloration and
557 behavioural syndromes. *Trends Ecol. Evol.* **23**, 502–510 (2008).
558 45. K. Hayashi, K. Tachihara, J. D. Reimer, Patterns of coexistence of six anemonefish
559 species around subtropical Okinawa-jima Island, Japan. *Coral Reefs* **37**, 1027–1038
560 (2018).
561 46. P. Salis, T. Lorin, V. Laudet, B. Frédérich, Magic traits in magic fish: understanding
562 color pattern evolution using reef fish. *Trends Genet.* **35**, 265–278 (2019).
563 47. H. Dong, *et al.*, Transient Maternal Hypothyroxinemia Potentiates the Transcriptional
564 Response to Exogenous Thyroid Hormone in the Fetal Cerebral Cortex Before the
565 Onset of Fetal Thyroid Function: A Messenger and MicroRNA Profiling Study. *Cereb.*

Cortex **25**, 1735–1745 (2015).
48. M. L. Berumen, *et al.*, Otolith geochemistry does not reflect dispersal history of clownfish larvae. *Coral Reefs* **29**, 883–891 (2010).
49. K. P. Burnham, D. R. Anderson, *Model selection and multimodel inference* (Springer-Verlag New York, 2002).
50. M. R. E. Symonds, A. Moussalli, A brief guide to model selection, multimodel inference and model averaging in behavioural ecology using Akaike's information criterion. *Behav. Ecol. Sociobiol.* **65**, 13–21 (2011).
51. H. Schielzeth, Simple means to improve the interpretability of regression coefficients. *Methods Ecol. Evol.* **1**, 103–113 (2010).
52. K. Bartoń, MuMIn: Multi-Model Inference, Version 1.43.6. *R Packag.* (2019).
53. R Core Team (2020), R: A language and environment for statistical computing. *R A Lang. Environ. Stat. Comput. R Found. Stat. Comput. Vienna, Austria* (2020).
54. D. M. Parichy, M. R. Elizondo, M. G. Mills, T. N. Gordon, R. E. Engeszer, Normal table of postembryonic zebrafish development: Staging by externally visible anatomy of the living fish. *Dev. Dyn.* **238**, 2975–3015 (2009).
55. D. S. Eom, E. J. Bain, L. B. Patterson, M. E. Grout, D. M. Parichy, Long-distance communication by specialized cellular projections during pigment pattern development and evolution. *Elife* **4** (2015).
56. J. E. Spiewak, *et al.*, Evolution of Endothelin signaling and diversification of adult pigment pattern in Danio fishes. *PLOS Genet.* **14**, e1007538 (2018).

Figure legends

Figure 1. Formation of white bars of *Amphiprion percula* new recruits is differentially influenced by age depending on the anemone species

(A-B) Histograms representing percentage of new recruits having 1 (blue), 2 (green) or 3 white bars (yellow) depending on their age, in new recruits living in *H. magnifica* (A) or *S. gigantea* (B). Statistical tests were done using χ^2 tests at each age between *H. magnifica* or *S. gigantea* and show statistical difference at 150-200 dph and 200-250 dph (respective p-value: 0.0032 and 0.0011). (C) Number of bars (85% CI) depending on age of individuals predicted from full averaging of the model candidates (D). Blue and orange represent respectively *A. percula* new recruits sampled in *H. magnifica* and in *S. gigantea*. Dots are observed data and are shifted around their number of bars for graphical representation. Predicted regressions of the number of bars are presented for the reference level “lagoon 0”. (D) Full model averaged estimates (85% CI) of linear regression parameters from models including age for each anemone species. Parameter estimates after model averaging of treatment were compared with “Lagoon 1” as reference for the geographic zone. A parameter estimate whose 85% CI includes zero is considered uncertain and parameter estimates whose 85% CI do not overlap are considered different.

Figure 2. Adult color pattern formation in *Amphiprion ocellaris* is linked to a switch in expression of pigment cells specific genes during post-embryonic development

(A-B) Stereomicroscope images of entire larvae and the associated zoom of the trunk at stage 1 (A), 2 (B), 3 (C), 4 (D), 5 (E), 6 (F) and 7 (G) (Adapted from (25)). White and red arrowheads point white bars and black larval melanophores, black and orange arrows point respectively melanophores and xanthophores. (H and I) PCA analysis of the pigmentation genes (H) and iridophores genes (I) expression from transcriptomic analysis from entire larvae over post-embryonic stages. The two PCA exhibit a clear separation between stage 1 to 3 and stage 4 to 7. The ellipses were arbitrarily drawn around arrays to help resolution: stages 1 to 3 (orange) and 4 to 7 (blue) arrays. All stages had 3 replicates. (J) Heatmap of the 7 iridophore genes having the highest fold change between stage 1-3 and stages 5-7. Color represents the intensity of the centered (but unscaled) signal that goes, for each gene, from low (blue) to medium (white) to high (red).

Figure 3. White bars in *Amphiprion ocellaris* form earlier and later respectively after treatments with thyroid hormones or goitrogens

(A-D) Stereomicroscope images of larvae treated at stage 3 during 3 days (dpt) in DMSO (A) or T3 at 10^{-6} M (B), 10^{-7} M (C) and 10^{-8} M (D).

(E-F) Histogram showing the percentage of larvae having 0 (red), 1 (blue), 2 (green) or 3 (yellow) white bars. (E) Larvae are treated at stage 3 for 3 days with DMSO, T3 10^{-6} M, 10^{-7} M and 10^{-8} M (nDMSO=16, nT3 10^{-8} M=20, nT3 10^{-7} M=18, nT3 10^{-6} M=15 individuals). Chi2 tests are significant between T3 10^{-6} M and DMSO (p-value <0.0001). (F) Larvae are treated at stage 3 for 9 days with DMSO or MPI 10^{-6} M (nDMSO=12, nMPI 10^{-6} M= 13 individuals). Statistical test was done using χ^2 tests (p-value <0.0029).

(G-I) Stereomicroscope images of larvae treated at stage 3 during 9 days in DMSO (G) and MPI 10^{-6} M (H) and MPI 10^{-6} M stage 3 larvae treated for 25 days (I).

(J) Graphic showing the number of melanophores in a specific area of the trunk in DMSO (black), T3 10^{-6} M (green) and MPI 10^{-6} M (red) at 12, 24, 48 and 72 hpt (nDMSO>9, nT3>9, nMPI>9 individuals). Statistical tests were done using ANOVA between the T3 or MPI treatments and DMSO (control) at each time. Tests are significant between T3 and DMSO at 48 hpt and 72 hpt (p-value are respectively equal to 0.0299 and 0.0043).

Bars correspond to the mean and crosses correspond to one experiment. hpt = hours post treatment. Scale bar = 1mm.

Figure 4. *duox* requirement for the timing of color pattern formation in zebrafish

(A) Graph representing T3 level (in pg.g-1 of fish) in *A. percula* new recruits sampled in *H. magnifica* or *S. gigantea* (Non-parametric Mann Whitney Test, p-value=0.0022). (B) Volcano plot of differentially expressed genes between new recruits living in *H. magnifica* or *S. gigantea*. Positive Log2FC values correspond to an increased expression in recruits from *S. gigantea*, while negative Log2FC corresponds to increased expression in recruits from *H. magnifica*. Green and red points correspond to significantly differentially expressed genes. The vertical black lines delimit the Log2FC threshold of 1, while the horizontal line corresponds to the corrected p-value threshold. (C) Inverted fluorescence images show iridophores (dark cells) marked by *pnp4a:mem-mCherry* expression at 10.6 mm standard in wild-type (left) and *duox* CRISPR/Cas9 mutants (Right). (D) Numbers of interstripes were scored qualitatively over Standard Length (SL) in wild-type (blue, N=61) and *duox* CRISPR/Cas9 mutants (yellow, N=51). Complete interstripes received a score of 1 and developing interstripes received a score of 0.5. Each circle represents a single individual and points are jittered vertically for clarity, and equivalently smoothed splines are shown for ease of visualization. Differences in total numbers of interstripes and tractories of interstripe addition resulted in significant effects of genotype (likelihood ratio test, χ^2=91.7, p-

661 value<0.0001, d.f. = 1) and genotype x standard length interaction (χ^2=21.9, p-value<0.0001,
662 d.f. = 1). (E) Despite having fewer interstripes overall, *duox*-deficient animals had
663 proportionally more of the flank covered by dense, interstripe-iridophores, as compared to
664 the wild type ($F_{1,43}$=76.1, P<0.0001). Bars indicate means ± 95% confidence intervals. Scale
665 bar in A = 200 μm.

666

667

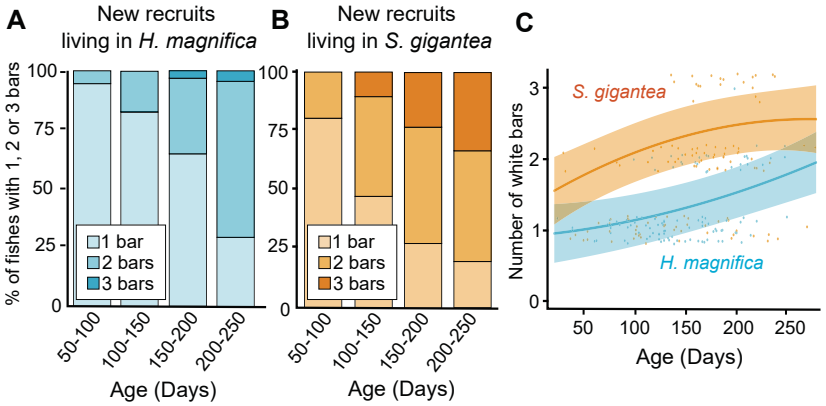

D

	H. magnifica		*S. gigantea*	
Parameter	Averaged β	85% C.I.	Averaged β	85% C.I.
Intercept	1.28	1.214; 1.345	1.511	1.393; 1.629
Age	0.067	-0.086; 0.35	0.481	0.108; 0.89
Age2	0.123	0.024; 0.351	-0.268	-0.774; -0.016
N_Fish	-0.037	-0.207; 0.026	-0.205	-0.307; -0.125
Female size	0.017	-0.02; 0.115	-0.015	-0.173; 0.069
Length difference	-0.003	-0.108; 0.084	0.023	-0.04; 0.177
Depth	-0.003	-0.077; 0.051	-0.006	-0.099; 0.056
Lagoon2	-0.002	-0.17; 0.124	0.667	0.478; 0.857
Lagoon3	-0.001	-0.168; 0.155	0.246	0.062; 0.43

Salis et al. Fig 1

Salis et al.,
Fig 2

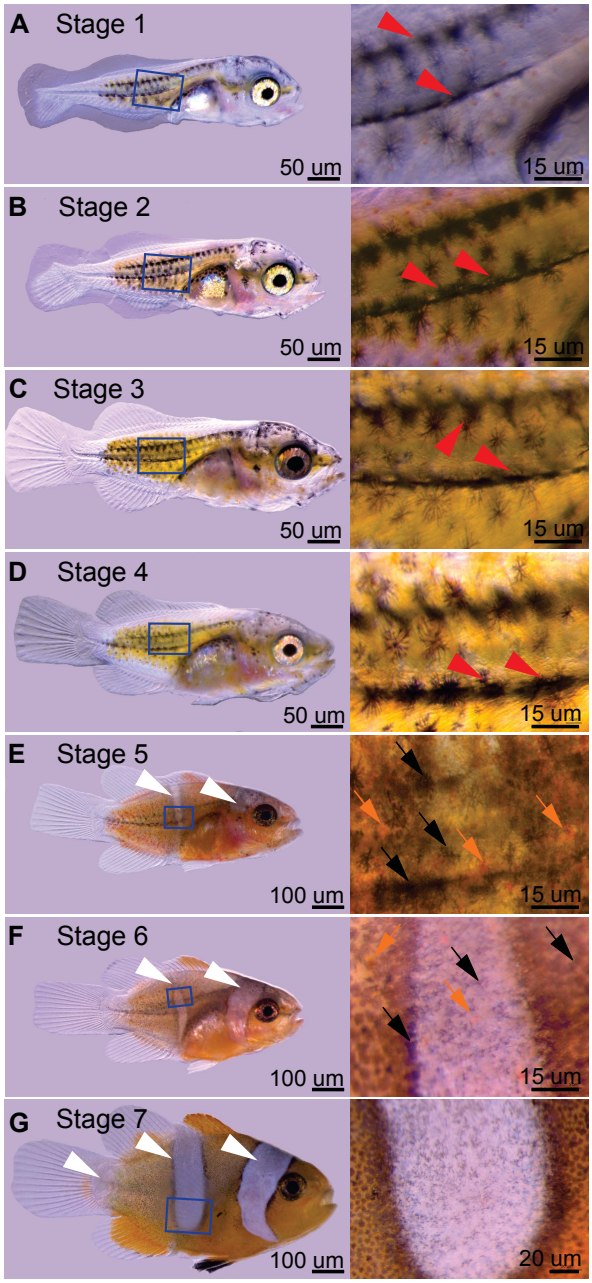

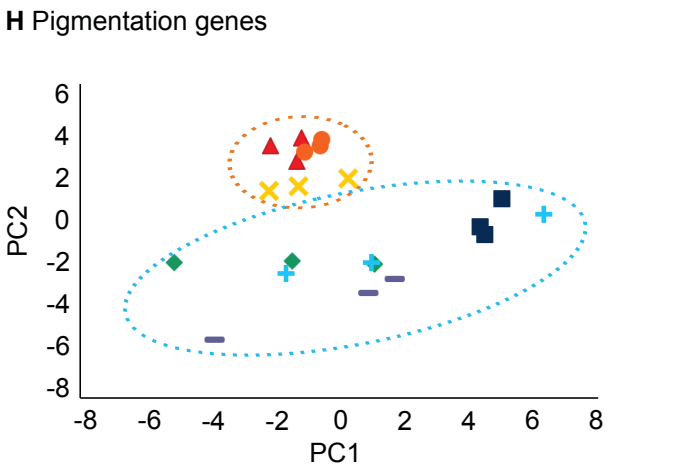

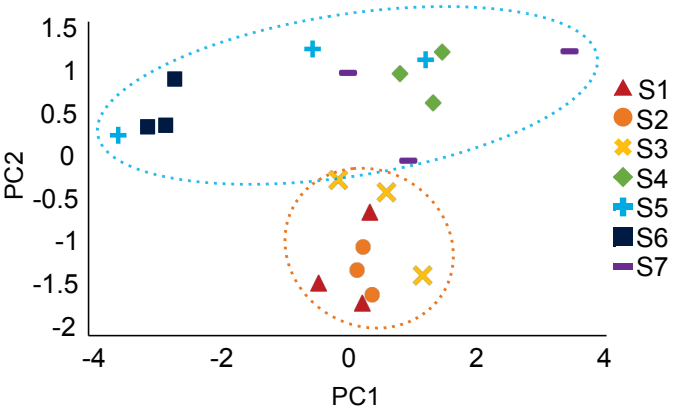

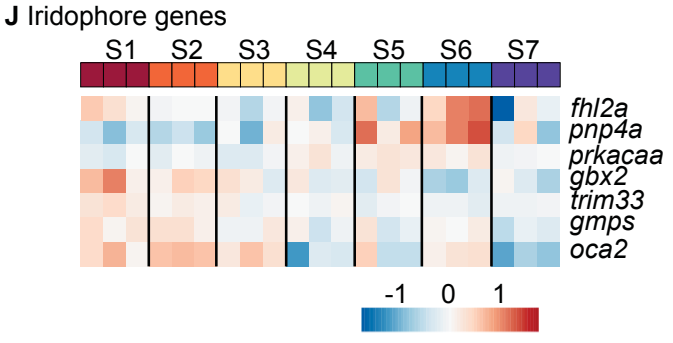

Salis et al.,
Fig 3

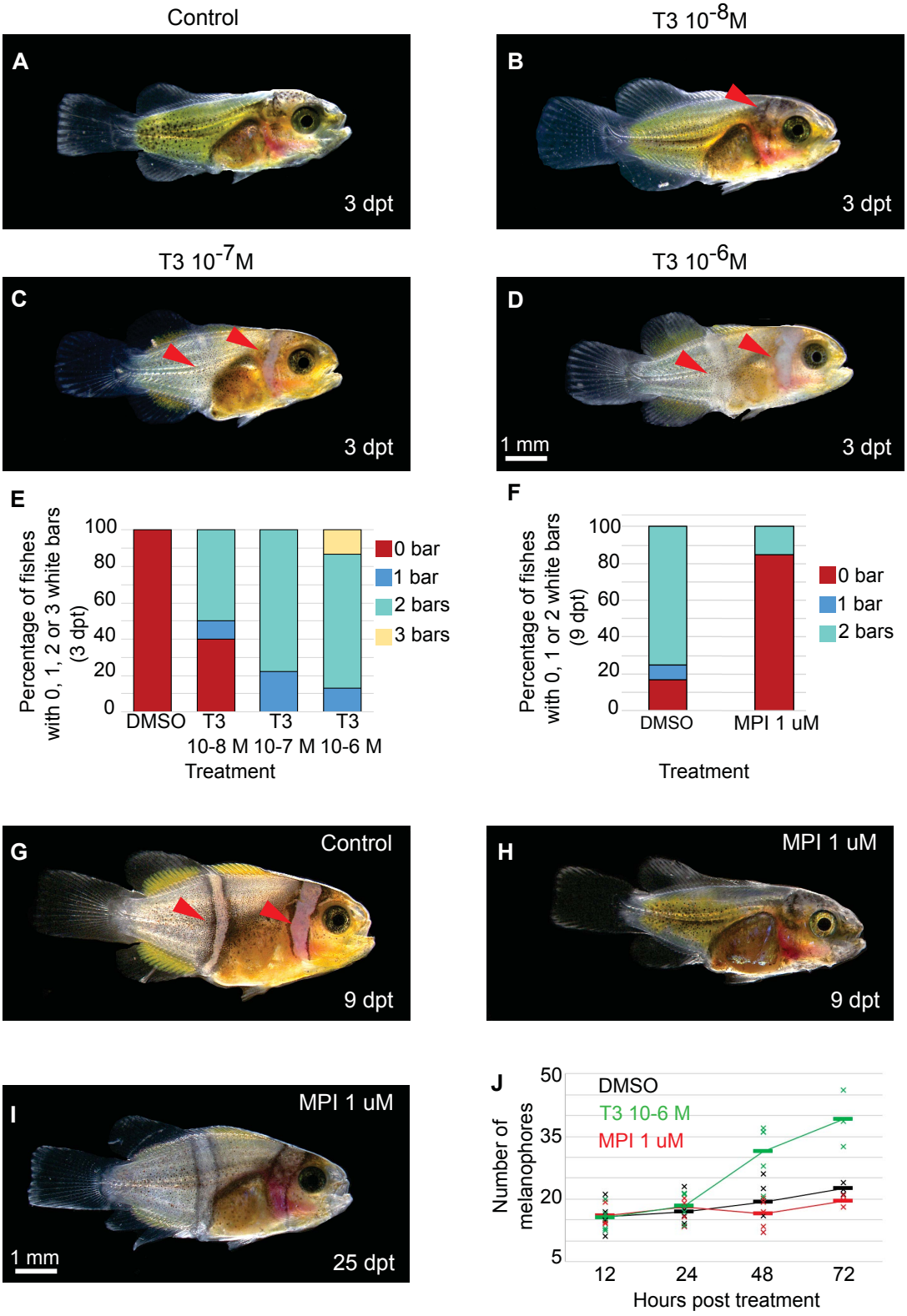

Salis et al.,
Fig 4